Case Studies in Thermal Engineering 78 (2026) 107695

Contents lists available at ScienceDirect

Case Studies in Thermal Engineering

journal homepage: www.elsevier.com/locate/csite

Analytical modeling of grout heat storage effects in thermal response tests: Toward faster and more reliable parameter estimation

Hsiang-Wen Wang [a], Ying-Fan Lin [a,*], Chia-Hao Chang [b], Bo-Tsen Wang [b], Hikari Fujii [c], Yu-Feng Forrest Lin [d], Kuo-Hsin Yang [e], Jui-Pin Tsai [b,*]

[a] Department of Civil Engineering, Chung Yuan Christian University, Taoyuan, Taiwan
[b] Department of Bioenvironmental Systems Engineering, National Taiwan University, Taipei, Taiwan
[c] Graduate School of International Resource Sciences, Akita University, Akita, Japan
[d] Illinois State Geological Survey, University of Illinois at Urbana-Champaign, Champaign, USA
[e] Department of Civil Engineering, National Taiwan University, Taipei, Taiwan

GRAPHICAL ABSTRACT

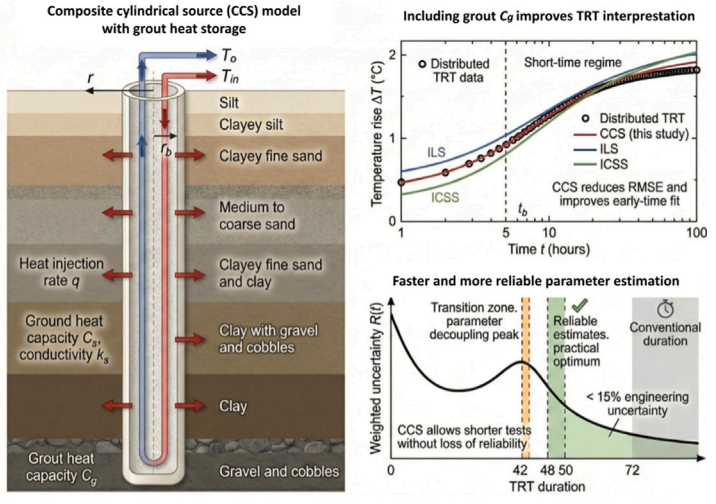

The proposed CCS model embeds grout heat capacity, improving the thermal response test (TRT) interpretation and enabling reliable parameter estimation with 48-50 h of data instead of 72 h.

ARTICLE INFO

Keywords:
Thermal response test

ABSTRACT

Accurate estimation of subsurface thermal properties is essential for the efficient design of ground-source heat pump (GSHP) and underground thermal energy storage (UTES) systems.

* Corresponding author.
E-mail addresses: yflin1110@cycu.edu.tw (Y.-F. Lin), jptsai@ntu.edu.tw (J.-P. Tsai).

https://doi.org/10.1016/j.csite.2026.107695
Received 26 October 2025; Received in revised form 8 January 2026; Accepted 9 January 2026
Available online 10 January 2026

Grout heat capacity
Ground source heat pump
Borehole heat exchanger
Analytical solution

However, conventional analytical models for thermal response tests (TRTs), such as the infinite line-source (ILS) and infinite cylindrical-surface-source (ICSS) solutions, neglect grout heat storage, leading to systematic bias during early heating periods. This study develops an analytical composite cylindrical source (CCS) model that explicitly accounts for the volumetric heat capacity of the grout (defined generically herein to denote borehole filling materials, including silica–sand backfill). The closed-form formulation reproduces Laplace-transform finite-difference simulations within 0.1 °C and demonstrates excellent agreement with a distributed TRT conducted on a 54 m borehole. The CCS model reduces the root-mean-square error from 0.163 °C (ILS) to 0.116 °C, resolves meter-scale stratification, and yields practically stable estimates of thermal conductivity and heat capacity using 48–50 h of data. A Bayesian uncertainty analysis reveals a 'transition zone' around 42 h, suggesting that tests should extend beyond this period to avoid false convergence, but need not extend to 72 h for engineering purposes. Sensitivity analysis indicates that grout heat capacity governs early-time temperature response, whereas ground conductivity dominates later stages. The results show that incorporating grout heat storage significantly improves TRT interpretation accuracy and allows test duration to be shortened without compromising reliability, offering a practical framework for field-scale thermal characterization in GSHP design.

1. Introduction

The rising demand for sustainable energy has increased interest in underground thermal energy storage for long-term thermal management [1]. Common applications include district heating, industrial site heat recovery, and ground source heat pumps, which rely on subsurface thermal exchange [2,3]. Borehole thermal energy storage and ground source heat pumps are of particular interest due to their use of stable underground temperatures for heating and cooling [4,5]. System performance depends on the borehole heat exchanger (BHE), which transfers heat between the circulating fluid and the ground [6]. Accurate estimation of key BHE thermal parameters, such as thermal conductivity and volumetric heat capacity, is essential for optimizing borehole thermal energy storage and ground source heat pump performance, as these parameters control subsurface heat transfer efficiency [7,8].

The thermal response test (TRT) has become the standard in-situ method for estimating subsurface thermal properties by applying a constant heat load to the circulating fluid within a BHE and analyzing the temperature response over time [9,10]. Mogensen [11] was the first to apply the infinite line source (ILS) model, originally developed by Jaeger and Carslaw [12], to interpret TRT data. The ILS model, widely adopted due to its computational simplicity and analytical tractability [13], relies on idealized assumptions, including an infinitesimally small borehole radius and uniform heat flux. The infinite cylindrical surface source (ICSS) model incorporates the effect of finite borehole radius to characterize radial temperature decay in cylindrical coordinates [14]. Although the ICSS model represents the borehole geometry more faithfully [15], its added complexity and continued neglect of grout thermal properties can degrade early-time fits [16,17]. Practitioners therefore still rely on the ILS model for short-duration interpretation even though it omits finite-radius effects. Additional analytical solutions have been developed to address varying boundary conditions and configurations, including the moving line source model for groundwater advection [18] and the finite line source model for surface temperature influence [19–21]. These solutions target longer operation periods, whereas short-duration TRTs typically experience negligible groundwater or surface effects [15]. Consequently, the ILS and ICSS models remain the most widely used for interpreting TRT data.

Despite these advancements, existing analytical models often neglect the thermal properties of the grout or backfill material [22], which significantly influence the early-time temperature response during TRT [23,24]. Previous studies have addressed this limitation by modeling TRT as a two-zone problem, solving separate partial differential equations (PDEs) for the grout and the ground [25–27]. Approaches based on Green's functions [25] or numerical models [28] have also been used to better approximate the actual TRT configuration. However, these methods often result in complex integral expressions or require numerical time-stepping schemes that lack the unified G-function structure familiar to practitioners. Consequently, they are less computationally efficient for inverse analysis compared to closed-form solutions and are difficult to integrate with standard optimization algorithms.

To address this limitation, a composite cylindrical source (CCS) model is developed, incorporating grout (or backfill) heat capacity directly into the inner-boundary condition of the TRT formulation. The resulting closed-form solution can be expressed as a modified G-function, allowing direct integration into existing design charts and simulation tools used by ground-source heat pump practitioners, while maintaining analytic efficiency. The CCS G-function is verified against Laplace-domain finite-difference results, benchmarked against the classical ILS and ICSS models, and subjected to [29] sensitivity analysis to identify the most influential thermal properties over time. A field application at National Taiwan University further demonstrates that stable parameter estimates can be achieved from substantially shorter TRT records when using the CCS formulation.

2. Methods

Methods comprise four components: derivation of the composite cylindrical source solution, numerical and experimental validation, global sensitivity analysis, and field deployment on a distributed TRT. Each subsection details one component so that the analytical development, benchmarking, and application steps can be followed sequentially.

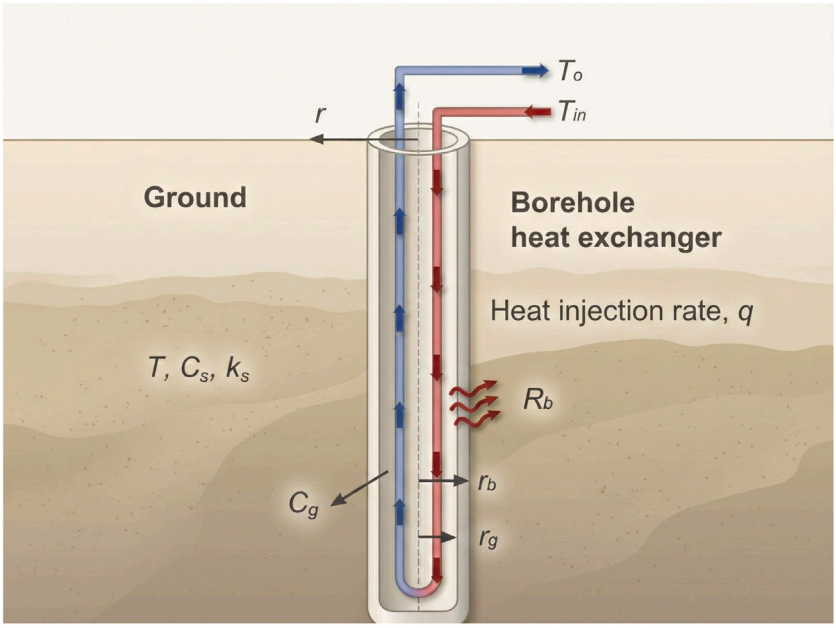

Fig. 1. Schematic diagram of the borehole heat exchanger in the proposed model for thermal response test.

2.1. Model development and analytical solution

The borehole heat exchanger configuration is illustrated in Fig. 1 within a homogeneous ground that extends infinitely in the vertical direction. The BHE is modeled as a cylindrical surface source with a constant heat injection rate, q (W/m), and a finite borehole radius, r_b (m). Because temperature is assumed to vary only with radial distance from the borehole wall, rather than with depth or azimuthal angle, the full three-dimensional conduction problem collapses to a single radial dimension. The governing equation therefore becomes

$$C_s \frac{\partial T}{\partial t} = k_s \frac{1}{r} \frac{\partial}{\partial r}\left(r \frac{\partial T}{\partial r}\right), \quad (r,t) \in [r_b, \infty) \times [0, \infty), \tag{1}$$

where T is the uniform temperature (°C) in the ground, r is the radial distance from the center of the borehole (m), and t is time (s). The parameter C_s denotes the volumetric heat capacity of the ground (J m^{-3} °C^{-1}), and k_s is the thermal conductivity of the ground (W m^{-1} °C^{-1}). We assume an undisturbed ground temperature T_0 (°C), giving the initial condition:

$$T|_{t=0} = T_0. \tag{2}$$

At the borehole surface, an energy balance is applied to account for thermal storage within the borehole. Although many TRT applications use cementitious grout, the field site examined here employs a silica–sand-based fill material. For consistency with conventional TRT terminology, this material is hereafter referred to as "grout". The boundary condition at $r = r_b$ is therefore:

$$2\pi r_b k_s \left.\frac{\partial T}{\partial r}\right|_{r=r_b} = -q + \pi r_b^2 C_g \left.\frac{\partial T}{\partial t}\right|_{r=r_b}, \tag{3}$$

where C_g is the volumetric heat capacity of the grout (i.e., our silica–sand-based backfill) (J m^{-3} °C^{-1}). At an infinite radial distance, we impose:

$$\left.\frac{\partial T}{\partial r}\right|_{r\to\infty} = 0. \tag{4}$$

Applying the Laplace transform to these equations yields

$$C_s\left(s\bar{T} - T_0\right) = k_s \frac{1}{r} \frac{d}{dr}\left(r \frac{d\bar{T}}{dr}\right), \tag{5a}$$

$$2\pi r_b k_s \left.\frac{d\bar{T}}{dr}\right|_{r=r_b} = -\frac{q}{s} + \pi r_b^2 C_g\left(s\bar{T}|_{r=r_b} - T_0\right), \tag{5b}$$

and

$$\left.\frac{d\bar{T}}{dr}\right|_{r\to\infty} = 0, \tag{5c}$$

Table 1
Comparison of existing analytical solutions and their inner boundary conditions.

Analytical solution	Inner boundary condition
Infinite line source (ILS) [35]	$2\pi r k_s \frac{\partial T}{\partial r}\Big\|_{r\to 0} = -q$
Infinite cylindrical surface source (ICSS) [35]	$2\pi r k_s \frac{\partial T}{\partial r}\Big\|_{r=r_b} = -q$
composite cylindrical source (CCS) (This study)	$2\pi r_b k_s \frac{\partial T}{\partial r}\Big\|_{r=r_b} = -q + \pi r_b^2 C_g \frac{\partial T}{\partial t}\Big\|_{r=r_b}$

where the overbar denotes that the function is expressed in the Laplace domain, and s is the Laplace variable.

Solving Eq. (5a) subject to the boundary conditions (5b)–(5c) gives:

$$\bar{T} = \frac{q\,K_0(\lambda r)}{\pi r_b^2 C_g s^2 K_0(\lambda r_b) + 2 k_s \pi r_b s \lambda K_1(\lambda r_b)} + \frac{T_0}{s}, \tag{6a}$$

with

$$\lambda = \sqrt{\frac{s C_s}{k_s}}. \tag{6b}$$

Unlike composite (multi-zone) TRT models that solve separate PDEs for the grout and formation, thereby requiring coupled numerical solutions or complex eigenvalue expansions, we embed grout heat storage as a lumped capacity in a dynamic Robin boundary condition at $r = r_b$ (Eq. (5b)). This formulation reduces the problem to a single-domain equation, yielding a tractable closed-form solution akin to the classical line source but with a modified kernel. As validated against the rigorous two-zone finite difference benchmark in Section 2.2 (Fig. 3), this lumped approach reproduces the full radial gradient behavior with negligible error for standard borehole geometries, effectively balancing physical accuracy with analytical efficiency. The grout enters only through the extra $C_g s^2$ term in the denominator of Eq. (6a), recovering ILS/ICSS as $C_g \to 0$. Consistent with standard TRTs, we prescribe a line heat rate q and do not resolve an in-tube transfer model; if a mean fluid temperature is needed, it can be obtained a posteriori via a borehole/tube resistance, in line with classic practice [30,31].

The inverse Laplace transform of Eq. (6a) gives the time-domain solution:

$$T = \frac{2 q \eta}{\pi^2 k_s} \int_0^\infty \frac{\left(1 - e^{-\beta^2/4 u_b}\right)\delta}{\beta^2 \Delta(\beta)}\, d\beta + T_0, \tag{7a}$$

where

$$\eta = \frac{C_s}{C_g}, \quad u_b = \frac{C_s r_b^2}{4 k_s t}, \tag{7b}$$

$$\delta = J_0\!\left(\frac{\beta r}{r_b}\right)\left[\beta Y_0(\beta) - 2\eta Y_1(\beta)\right] - Y_0\!\left(\frac{\beta r}{r_b}\right)\left[\beta J_0(\beta) - 2\eta J_1(\beta)\right], \tag{7c}$$

$$\Delta(\beta) = \left[\beta J_0(\beta) - 2\eta J_1(\beta)\right]^2 + \left[\beta Y_0(\beta) - 2\eta Y_1(\beta)\right]^2, \tag{7d}$$

This solution shares a similar analytical form to that presented in Papadopulos and Cooper [32] for well hydraulics problems.

The temperature at the borehole surface, $T(r_b, t)$, follows by setting $r = r_b$ in Eq. (7a):

$$T(r_b, t) = \frac{q}{k_s} \frac{8\eta^2}{\pi^3} \int_0^\infty \frac{\left(1 - e^{-\beta^2/4 u_b}\right)}{\beta^3 \Delta(\beta)}\, d\beta + T_0. \tag{8}$$

Although this expression contains an improper integral, it can be evaluated very efficiently by numerical quadrature: mapping $(0, \infty)$ to a finite interval and using high-accuracy rules (e.g., double-exponential/tanh–sinh or Gauss–Laguerre) or adaptive infinite-interval routines (e.g., QUADPACK QAGI) yield geometric (often exponential) convergence to the prescribed tolerance, making the computation both robust and fast [33].

Finally, the mean temperature of the fluid from the CCS model, T_f, includes the effect of borehole thermal resistance:

$$T_f = T(r_b, t) + q R_b, \tag{9}$$

where R_b is the effective borehole thermal resistance. Following [34], one can define:

$$R_b = \frac{1}{2\pi k_g} \ln\!\left(\frac{1}{\sqrt{n}}\right), \tag{10}$$

with k_g denoting the thermal conductivity of the grout (i.e., silica–sand fill in our field site), and n the number of pipes in the borehole. In addition, we summarize inner boundary conditions used in the ILS, ICSS, and proposed CCS models in Table 1.

2.2. Model validation

To validate the analytical solution derived in this study, a numerical solution is constructed using a Laplace transform finite difference (LTFD) method coupled with the Stehfest inversion algorithm [36] applied to Eq. (5). One key advantage of the LTFD method is that the traditional stability and accuracy issues associated with discretization of the time derivative in transient analyses become irrelevant, as the time derivative is not explicitly discretized. Consequently, LTFD allows an unlimited time step size without loss of accuracy, offering superior accuracy and stable, non-increasing round-off error. This approach significantly reduces computational efforts, typically requiring only one numerical inversion step, as opposed to multiple time-stepping procedures employed by conventional finite difference methods [37].

A uniform radial mesh discretization scheme is adopted, dividing the domain from the borehole radius r_b to an outer radius $R_{\max}$ into N segments, resulting in $N+1$ nodes. The radial coordinate at each node is defined as:

$$r_i = r_b + i\frac{R_{\max} - r_b}{N}, \quad i = 0, 1, \ldots, N \tag{11}$$

The finite difference discretization of the governing equation at an internal node i is given by:

$$a_i \bar{T}^{i-1} + b_i \bar{T}^{i} + c_i \bar{T}^{i+1} = 0, \quad 1 \le i \le N-1 \tag{12}$$

with coefficients defined as:

$$a_i = \frac{k_s}{\Delta r^2} - \frac{k_s}{2r_i \Delta r}, \quad b_i = -\frac{2k_s}{\Delta r^2} - C_s s, \quad c_i = \frac{k_s}{\Delta r^2} + \frac{k_s}{2r_i \Delta r} \tag{13}$$

At $r = r_b$ ($i = 0$), the inner boundary condition is discretized as:

$$\left(2\pi r_b k_s \frac{\bar{T}^1 - \bar{T}^0}{\Delta r}\right) = -\frac{q}{s} + \pi r_b^2 C_g s \bar{T}^0 \tag{14}$$

which rearranges to the following linear form:

$$(\phi_1 + \phi_2)\bar{T}^0 - \eta \bar{T}^1 = \frac{q}{s}, \quad \phi_1 = \frac{2\pi r_b k_s}{\Delta r}, \quad \phi_2 = \pi r_b^2 C_g s \tag{15}$$

At the outer boundary ($i = N$), a no-flux condition ($dT/dr = 0$) is applied as:

$$\bar{T}^N - \bar{T}^{N-1} = 0 \tag{16}$$

The resulting linear system is written in a compact matrix form as:

$$\mathbf{M}(s)\bar{\mathbf{T}}(s) = \mathbf{b}(s) \tag{17}$$

where $\mathbf{M}(s)$ is an $(N+1)\times(N+1)$ sparse coefficient matrix, $\bar{\mathbf{T}}(s)$ is the unknown nodal temperature vector in the Laplace domain, and $\mathbf{b}(s)$ is the corresponding right-hand-side vector. This linear system is solved efficiently using a sparse linear solver to obtain the solution $\bar{\mathbf{T}}(s)$.

To convert the transient temperature solution in the real-time domain, Stehfest algorithm can be employed for numerical inversion of the Laplace transform. The Stehfest inversion approximates the inverse Laplace transform via the following expression [36]:

$$T(r_b, t) \approx \frac{\ln 2}{t} \sum_{i=1}^{n} V_i \bar{T}\left(r_b, \frac{i \ln 2}{t}\right) \tag{18}$$

where the Stehfest weights V_i are calculated using factorial expressions.

The validity of the proposed CCS analytical solution is established through a two-stage verification process using consistent theoretical parameters: a borehole radius $r_b = 0.15$ m, ground thermal conductivity $k_s = 2.5$ W/m °C, ground volumetric heat capacity $C_s = 2.0 \times 10^6$ J/m^3 °C, initial temperature $T_0 = 13.0$ °C, and a heat injection rate $q = 50$ W/m.

First, the mathematical correctness of the closed-form derivation was verified against a LTFD solution. The verification considered three scenarios with varying heat capacity ratios ($\eta = C_s/C_g = 0.5, 1, 2$). As shown in Fig. 2, the CCS solution exhibits excellent agreement with the LTFD results across all scenarios (RMSE < 0.1 °C), confirming the accuracy of the analytical formulation and the numerical integration scheme.

Second, to assess the physical validity of the lumped-capacity assumption for the grout, the CCS model was benchmarked against a rigorous two-zone finite difference (FDM) model. Unlike the CCS formulation, the FDM explicitly resolves the radial temperature gradient within the grout ($0 \le r \le r_b$) and accounts for its finite thermal conductivity ($k_g = 1.8$ W/m °C). The FDM simulation employed a fully implicit time-stepping scheme to ensure stability, with the spatial domain discretized into a high-resolution grid (20 nodes in the grout, 100 nodes in the soil) to capture the steep temperature gradients near the borehole wall. Fig. 3(a) demonstrates that the temporal temperature evolution at the borehole wall and at radial distances of 0.30 m and 0.45 m matches the numerical benchmark with negligible deviation. Furthermore, the spatial profiles in Fig. 3(b) confirm that the CCS model accurately captures the temperature gradient near the borehole. This validates that the lumped-capacity simplification is physically robust for standard borehole configurations.

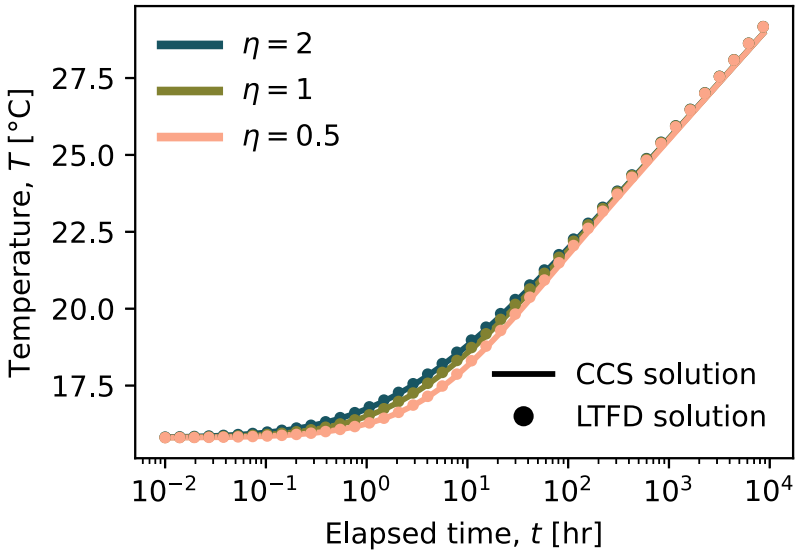

Fig. 2. Temporal distributions predicted by the proposed CCS solution and LTFD solution for η = 2, 1, and 0.5.

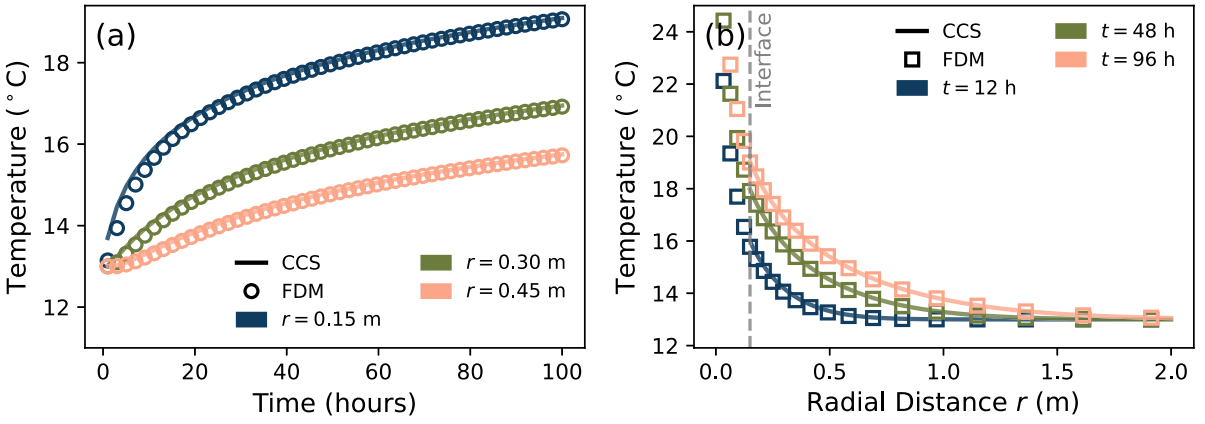

Fig. 3. Validation of the CCS analytical model against a rigorous Two-Zone FDM benchmark using consistent parameters (r_b = 0.15 m). (a) Temporal evolution at various radial distances. (b) Spatial temperature profiles at t = 12, 48, 96 h. The agreement confirms the validity of the lumped grout assumption.

2.3. Morris sensitivity analysis method

To quantify the influence of each parameter on the thermal response in space and time, the Morris screening method is applied [29]. Compared with variance-based approaches such as Sobol methods [38], Morris offers similar insight into non-linear and interaction effects while requiring significantly fewer model evaluations, providing a computationally efficient and sufficiently informative approach for the analyzed time window [39]. This global sensitivity analysis method perturbs one parameter at a time during sampling. The elementary effect for the kth aquifer parameter p_k (i.e., C_s, C_g, or k_s) is defined as

$$EE_k(t) = \frac{T(t; p_k + \Delta_\gamma) - T(t; p_k)}{\Delta_\gamma} \tag{19}$$

where Δ_γ refers to the sampling value in the interval $[1/(\gamma-1), \ldots, 1-1/(\gamma-1)]$, defined as $\Delta_\gamma = \gamma/2(\gamma-1)$ [29]. The variable γ represents the number of discrete and equally spaced values a parameter or variable can take within a defined interval.

Two statistical measures, the mean absolute elementary effect (μ^*) and standard deviation (σ), are employed to assess the sensitivity of the model to each parameter. Specifically, μ^* quantifies the average impact of changing a parameter across its range on the model output, indicating the overall effect of each parameter. Alternatively, σ measures the variability of these effects across different parameter levels, reflecting the presence of nonlinear interactions and dependencies between parameters on the model response [29].

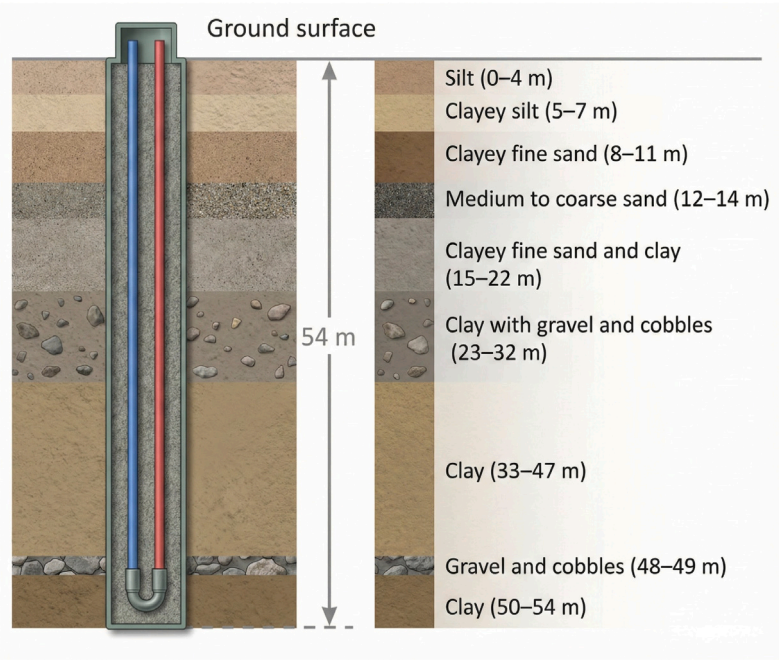

Fig. 4. Schematic of the borehole heat exchanger configuration (left) and the lithological column of the test site (right).

$$\mu_k^* = \frac{1}{N}\sum_{n=1}^{N} |EE_k^{(n)}| \tag{20a}$$

$$\sigma_k = \sqrt{\frac{1}{N-1}\sum_{n=1}^{N}\left[EE_k^{(n)} - \frac{1}{N}\sum_{n=1}^{N} EE_k^{(n)}\right]^2} \tag{20b}$$

The N is the total sampling number herein chosen to be 50. To assess the overall effect (denoted as χ), this study utilized the following measure to investigate the effect of a parameter on the thermal response:

$$\chi_k = \sqrt{\mu_k^{*2} + \sigma_k^2} \tag{21}$$

Accordingly, the values of χ_k should be greater than zero.

2.4. Field experimental setup

A field experiment on the National Taiwan University geothermal test field demonstrates the practical applicability of the proposed CCS solution. The test site (25.0143° N, 121.5401° E) covers approximately 100 m^2 and hosts a BHE constructed to a depth of 54 m using a vertically installed double-U configuration composed of high-density polyethylene (HDPE) pipes (DN25; outer diameter: 32 mm, inner diameter: 25 mm), selected for their high compressive strength, corrosion resistance, and ease of handling. Although many TRTs employ cementitious grout, the test well uses a silica sand-based fill at this site. For simplicity and consistency with standard TRT nomenclature, this fill is referred to as "grout" throughout this paper. Fiber optic cables are attached to the pipe surface and connected to an AP Sensing distributed temperature sensing (DTS) system (model N4385B), enabling continuous monitoring of subsurface temperature profiles during the TRT. For calibration, a double-ended configuration is implemented following the approach described by [40], using the CTEMPs MATLAB DTS Toolbox (https://ctemps.org/data-processing). The calibrated temperature accuracy is within ±0.1 °C. The spatial resolution is 1.0 m. The fiber was fixed securely to the depth-marked HDPE U-tube using cable ties and electrical tape, and depth tracking during installation yields an estimated depth-positioning uncertainty of approximately 0.1–0.2 m. Because the temperature profile is relatively uniform along depth, this positioning uncertainty has negligible impact on the thermal interpretation.

During drilling, ejected cuttings are collected and analyzed to construct a lithological column (Fig. 4). The stratigraphy is summarized as follows: from the surface to 14 m, interbedded fine sand and silt; from 15 to 22 m, alternating silt and clay; from 23 to 43 m, interbedded clay, silt, and gravel; from 33 to 47 m and 50 to 54 m, thick clay layers; and from 48 to 49 m, a gravel layer. Based on literature values, the saturated thermal conductivity of these materials typically ranges from 1 to 2 W/m °C [41–44].

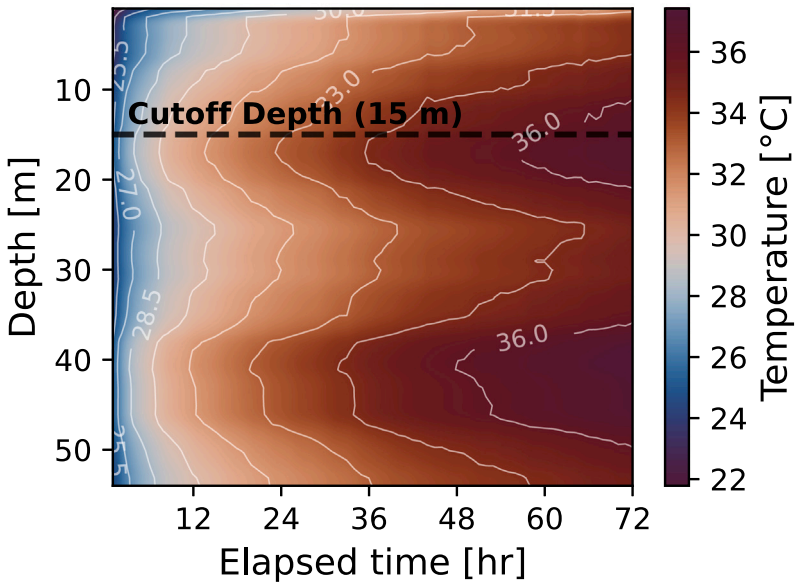

Fig. 5. Spatiotemporal temperature distribution along the borehole measured by DTS during the 72 h TRT. The dashed line marks 15 m depth, above which data are excluded from inversion due to seasonal surface-temperature influence.

Additionally, the thermal conductivity of the silica sand-based grout (k_g) is measured as 2.61 W/m °C using a KEM QTM-700 thermal property analyzer. These measurements anchor the inversion and keep the CCS-derived parameters physically realistic. Although the facies are interbedded, their saturated thermal conductivities fall within a narrow range (approximately 1–2 W m^{-1} °C^{-1}), with volumetric heat capacities that scale proportionally. At the meter-to-tens-of-meters scale relevant to radial heat diffusion during a TRT, these small contrasts act as an effective medium, so the bulk response can be represented by a single set of homogeneous parameters; the values obtained from the CCS inversion may therefore be regarded as equivalent thermal properties.

The TRT is conducted from 9 to 15 April 2024, applying a constant heat load of 2.5 kW with a circulating water flow rate of 15 L min^{-1} for 72 h, which is sufficient for the borehole and surrounding formation to approach near-equilibrium thermal conditions. Temperature profiles are continuously recorded to characterize the *in situ* thermal behavior of the BHE system. Vertical temperature profiles are also acquired using distributed temperature sensing (DTS) to evaluate the distribution of temperature changes along the borehole depth. The collected field data serve as a benchmark for validating the proposed CCS model, demonstrating how the analytical solution performs under realistic stratification before assessing shortened test durations. The spatiotemporal distribution of the recorded TRT data appears in Fig. 5. Elevated temperatures near the surface suggest potential influence from surface temperature fluctuations.

Based on the range of thermal properties reported in the literature for similar lithologies [41–44], a nominal thermal diffusivity of $\alpha \approx 8.33 \times 10^{-7}$ m^2/s was assumed. Using this value, the annual thermal damping depth was calculated as $d_{year} = \sqrt{2\alpha/\omega} \approx 2.89$ m, where ω is the angular frequency of the annual cycle. According to linear heat conduction theory, the amplitude of surface temperature fluctuations decays exponentially as $\exp(-z/d_{year})$, where z is the depth. Consequently, at a depth of $4d_{year}$ (≈ 11.6 m), the amplitude is attenuated to $e^{-4} \approx 1.8\%$ of the surface value. Therefore, a cutoff depth of 15 m was selected to conservatively exclude seasonal ambient temperature effects from the analysis.

To determine the thermal properties of ground (i.e., k_s and C_s), the differential evolution algorithm [45] is utilized for parameter estimation, aiming to minimize the discrepancy between observed temperature data and the analytical model predictions. The objective function is defined as the sum of squared residuals between the observed temperatures and those predicted by the proposed CCS model. Specifically, the parameters to be estimated are k_s, C_s, and C_g. The objective function, F_{obj}, is formulated mathematically as:

$$F_{\text{obj}} : \min_{k_s, C_s, C_g} \sum_{m=1}^{M} \left(T_{\text{sim}}^{(m)} - T_{\text{obs}}^{(m)} \right)^2, \tag{22}$$

where $T_{\text{sim}}^{(m)}$ is the simulated temperature at the mth measurement point, $T_{\text{obs}}^{(m)}$ is the observed temperature, and M represents the total number of observations.

The parameter bounds are carefully selected based on physically realistic ranges from the literature and engineering judgment. Parameter k is constrained between 0.1 and 5.0 W/(m °C), while C ranges from 1.0×10^6 to 9.0×10^6 J/(m^3 °C). Similarly, C_g falls between 1.0×10^5 and 9.0×10^6 J/(m^3 °C). The differential evolution optimization algorithm is implemented using the "best/1/bin" strategy, characterized by mutation factors ranging between 0.3 and 0.8 and a crossover probability of 0.6. This configuration

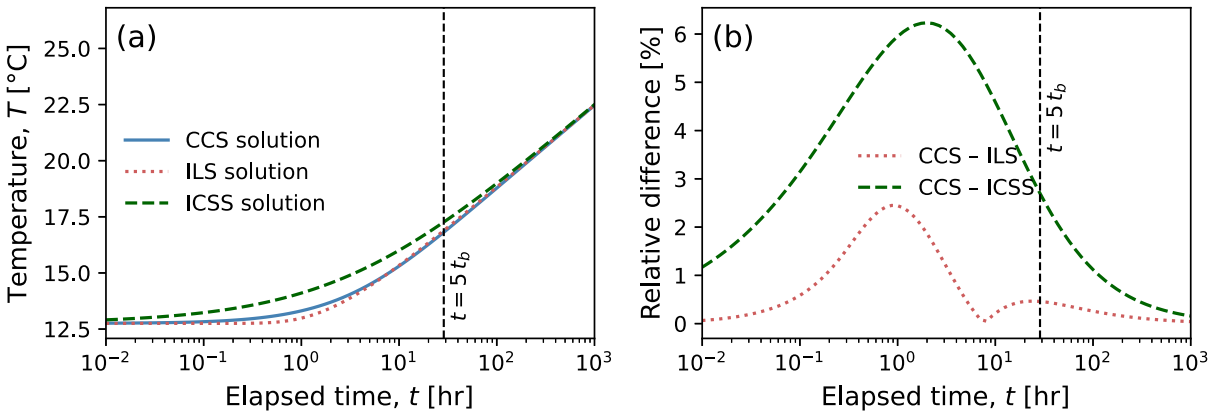

Fig. 6. (a) Temporal distributions of borehole temperature predicted by the proposed CCS kernel (Eq. (23)) and by the classical ILS (Eq. (24)) and ICSS (Eq. (25)) solutions, and (b) temporal distributions of relative difference with respect to the CCS solution. The dashed vertical line marks $t = 5\,t_b$, the upper bound of the short-time regime suggested by Li and Lai [15].

balances exploration and exploitation in the global search for optimal parameters. The population size and convergence criteria are carefully set to ensure the robustness of results and computational efficiency. The stochastic, population-based search of differential evolution diversifies trial solutions and thus helps the optimizer escape local minima, a property that has made differential evolution a standard choice for non-linear, multi-parameter inverse problems. Comparisons presented later in this study show that the resulting optimized parameters provide improved accuracy and robustness compared to existing analytical models (e.g., ILS and ICSS). The next subsection therefore evaluates the analytical solution against numerical benchmarks before comparing it with established TRT kernels.

3. Results and discussion

3.1. Comparison of existing solutions

The CCS kernel is benchmarked against the classical ILS and ICSS G-functions to quantify relative performance. In TRT studies it is customary to express the wall temperature rise as $qG(t)$, where the G-function isolates the transient ground response from the heating rate q [46]. Using this normalized form makes it easier to compare different analytical solutions and to scale results to arbitrary heat loads. For the present model, the G-function that includes grout (or backfill) heat capacity is

$$G_b(t) = \frac{1}{k_s}\frac{8\eta^2}{\pi^3}\int_0^\infty \frac{\left(1-e^{-\beta^2/4u_b}\right)}{\beta^3\,\Delta(\beta)}\,d\beta. \tag{23}$$

On the other hand, the G function of the classic ILS model can be expressed as:

$$G_{\mathrm{ILS}}(t) = \frac{1}{4\pi\,k_s}\mathrm{Ei}\left(\frac{r_b^2}{4\,\eta\,t}\right), \tag{24}$$

where $\mathrm{Ei}(\cdot)$ is the exponential integral function. The G function for the ICSS model is typically given by the integral form

$$G_{\mathrm{ICSS}}(t) = \frac{1}{2\pi\,k_s}\int_0^\infty \frac{1-\exp(-\eta\,\beta^2\,t)}{\beta}\,J_0\left(\beta\,r_b\right)\,d\beta, \tag{25}$$

in which $J_0(\cdot)$ denotes the Bessel function of the first kind of order zero. Both ILS and ICSS solutions ignore the volumetric heat capacity of the grout inside the borehole, leading to certain limitations for short-time/high-frequency thermal response analysis.

CCS predictions capture the short-time temperature evolution more accurately than the ILS and ICSS models, as illustrated in Fig. 6 using (a) semi-log and (b) log–log time scales. The vertical dashed line in each subplot marks $t = 5\,t_b$, where $t_b = r_b^2 C_g/k_s$ defines the short-time range in which grout heat capacity significantly influences the borehole temperature response [15].

Fig. 6(a) shows that prior to t around $5t_b$, the three solution predictions diverge: the ILS curve lies lowest, the ICSS highest, and the CCS result falls in between, closely tracking the measured temperatures. The lower ILS temperatures result from the neglect of grout heat storage in the model, while the elevated ICSS values stem from its finite-cylinder boundary condition which, in the absence of a capacity term, transfers more heat into the formation at early times. By explicitly incorporating grout volumetric heat capacity, the CCS model more accurately captures the initial temperature rise. Fig. 6(b) plots the relative difference $|\Delta T|/T_{\mathrm{CCS}}$ (%) between the CCS prediction and the two classical models. The discrepancy peaks when t is close to t_b, reaching about 2%–3% for the ILS curve and 6% for the ICSS curve. It then decays roughly as $1/\ln t$, falling below 1% once t exceeds $5\,t_b$.

This confirms that $t = 5\,t_b$ serves as a critical physical threshold delineating the short-time regime. Within this window ($t < 5\,t_b$), where grout heat capacity dominates the thermal response, the proposed CCS model provides the most significant accuracy

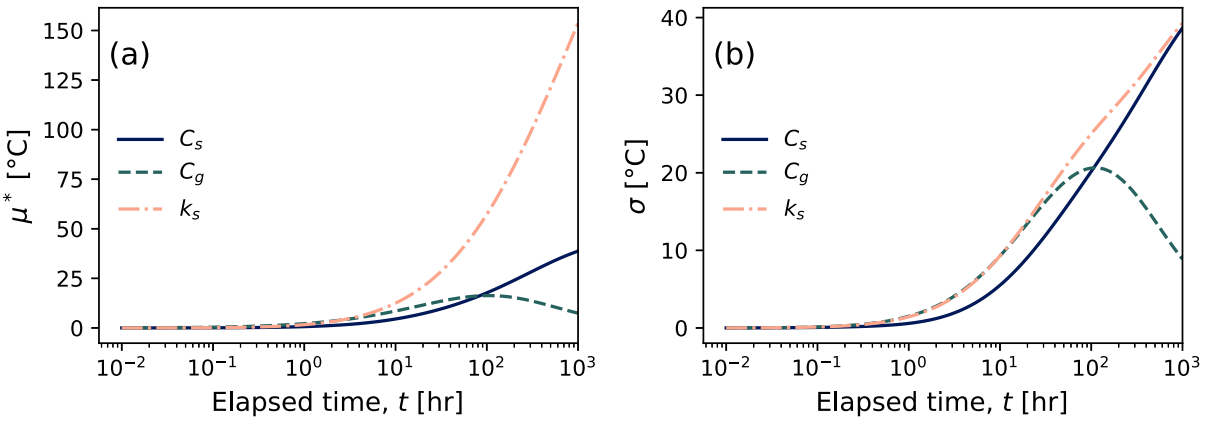

Fig. 7. Temporal distributions of (a) absolute elementary effect, μ^*, (Eq. (20a)) and (b) standard deviation, σ, (Eq. (20b)) for the parameters C_s, C_g, and k_s.

Table 2
Estimated parameters and RMSE against field data for the CCS, ILS, and ICSS solutions in the heating phase.

Solution	k_s (W/m ° C)	C_s (MJ/m^3 ° C)	C_g (MJ/m^3 ° C)	RMSE (° C)
CCS	1.00	2.30	1.60	0.12
ILS	1.20	1.44	–	0.16
ICSS	0.76	5.00	–	0.25

gain over conventional solutions. Beyond this threshold, the grout capacity effects diminish, and all models converge toward the formation-dominated behavior.

3.2. Results of sensitivity analysis

To investigate how the borehole temperature responds to variations in C_s, C_g, and k_s, a Morris global sensitivity analysis is conducted. As shown in Fig. 7a, μ^* for k_s rises sharply with increasing time, indicating that thermal conductivity increasingly dominates the overall temperature response at longer horizons. In contrast, C_g exerts a moderate influence in the early to intermediate periods but eventually diminishes in significance, as its short-term buffering effect on borehole temperature becomes less critical once the system transitions toward a more steady-state behavior. The parameter C_s maintains a non-negligible role throughout, with a gradual rise in μ^* from 10^2 hr to about 10^3 hr. Fig. 7(b) further illustrates these trends with the standard deviation σ, confirming that both k_s and C_s develop stronger nonlinear or interaction effects at late times, whereas C_g shows a pronounced but narrower influence window before leveling off. These findings imply that for short-term (hourly to daily) operation or design scenarios, one should pay close attention to both C_g and C_s.

3.3. Depth-averaged parameter estimation and uncertainty analysis

Parameter estimation was performed using the differential evolution algorithm on the 72-hour heating phase data, using the spatially averaged temperature across the entire borehole depth (15–54 m). This depth-averaged approach serves as a baseline to evaluate model accuracy and to determine the necessary test duration before analyzing stratigraphic details. Three analytical models were examined: (1) the proposed CCS solution, explicitly incorporating grout thermal capacity; (2) the ILS model; and (3) the ICSS model. During the 72-hour heating phase, three parameters were estimated for the CCS solution: k_s, C_s, and C_g. Table 2 summarizes the estimated parameter values along with the corresponding RMSE against the observation data from the field experiment. Overall, the CCS solution achieved the lowest RMSE (0.12 °C), confirming that explicitly modeling the grout thermal capacity improves short-term accuracy compared to existing analytical solutions.

The temporal distribution of temperature rise ($T - T_0$) predicted by the three models is shown in Fig. 8. The CCS curve closely matches the measured data, particularly at early times, and outperforms the ILS and ICSS models. The CCS solution reduces error by 50% relative to ICSS and by 25% relative to ILS, while avoiding the overestimation of k_s and underestimation of C_s caused by neglecting grout heat capacity.

Traditionally, a 72-hour duration is recommended for TRT [47,48], largely because most analytical interpretations rely on the late-time behavior of the ILS solution. To quantitatively evaluate the minimum required test duration for the proposed CCS model, we performed a Bayesian uncertainty analysis. We introduced a sensitivity-weighted relative uncertainty index, $R(t)$, to quantify the overall reliability of the parameter estimates weighted by their physical significance. Fig. 9 illustrates the evolution of the estimated parameters and the $R(t)$ index with increasing test duration.

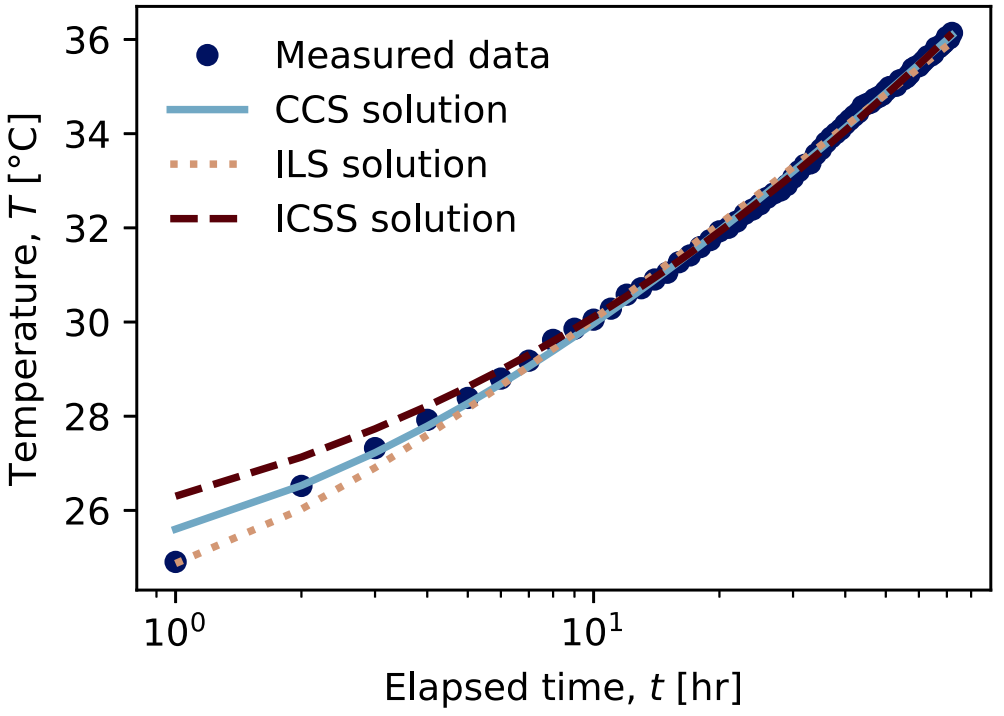

Fig. 8. Comparison of the measured temperature rise ($T - T_0$) predicted by the CCS solution (Eq. (23)), the ILS solution (Eq. (24)), and the ICSS solution (Eq. (25)) during the heating phase.

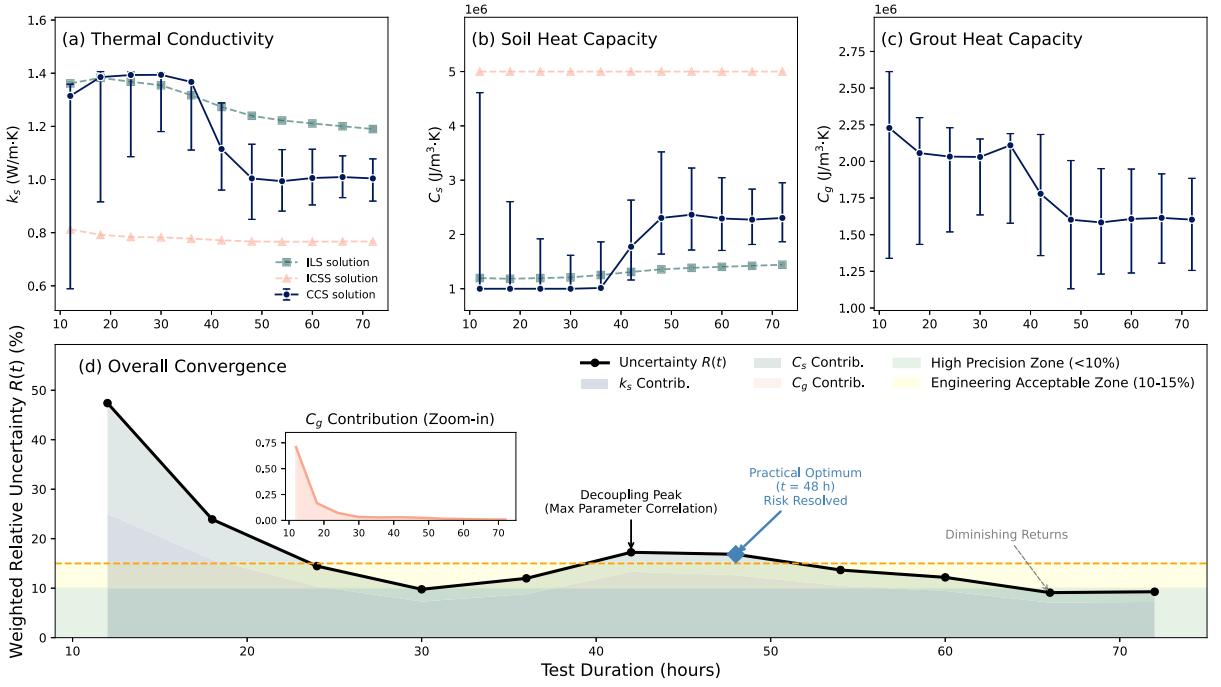

Fig. 9. Convergence of parameter estimation with truncated TRT duration. (a–c) Estimated values and 95% credible intervals for k_s, C_s, and C_g. (d) The sensitivity-weighted relative uncertainty index $R(t)$. The shaded areas represent the contribution of uncertainty from each parameter. Key features include a 'decoupling peak' at 42 h and a 'practical optimum' at 48 h.

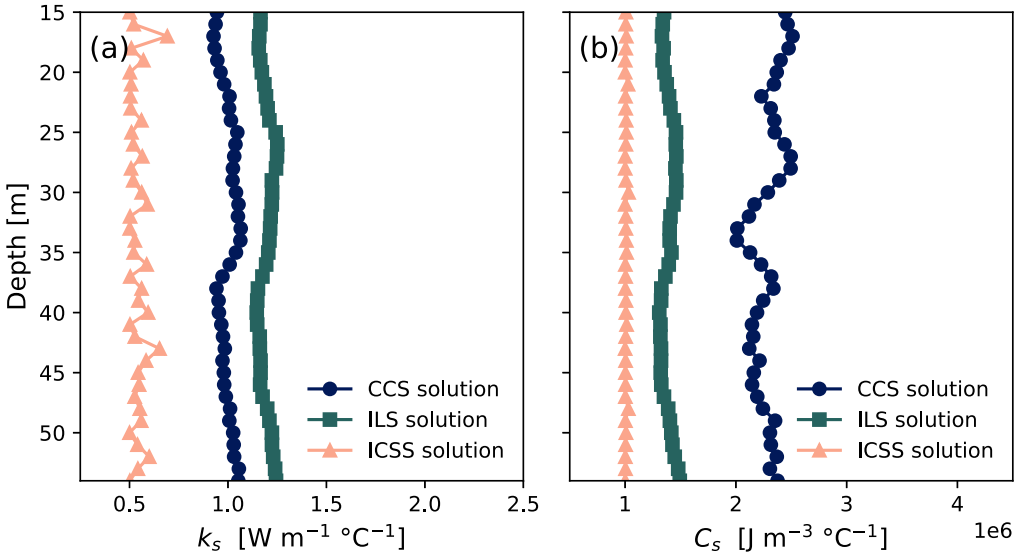

Fig. 10. Depth-resolved (a) thermal conductivity k_s and (b) volumetric heat capacity C_s inferred using the proposed CCS solution (Eq. (23)), ILS solution (Eq. (24)), and ICSS solution (Eq. (25)).

As shown in Fig. 9(d), the uncertainty evolution reveals a complex dynamic that challenges simple convergence criteria. The $R(t)$ index initially drops to a local minimum at $t = 30$ h, which might be mistaken for early convergence. However, this is followed by a sharp rebound, reaching a peak at $t \approx 42$ h. We identify this as the decoupling peak, corresponding to the physical transition where the heat pulse passes from the grout-dominated regime to the ground-dominated regime. During this transition, the parameter sensitivities overlap, maximizing the correlation and uncertainty.

Crucially, once the test duration exceeds this peak, the uncertainty decreases rapidly. At $t = 48$ h, $R(t)$ falls into the engineering acceptable zone ($< 15\%$). While extending the test to 66 h would further reduce $R(t)$ to below 10% (strict statistical convergence), the marginal improvement in parameter accuracy is minimal compared to the operational cost of the additional 18 h. Therefore, we identify 48–50 h as the practical optimal duration. This duration ensures that the analysis has robustly passed the high-risk transition zone and resolved the major trade-offs between grout and ground properties, thereby justifying a significant reduction in test duration without compromising engineering reliability.

3.4. Depth-resolved parameter estimation

Having established the accuracy and optimal duration of the CCS model based on depth-averaged behavior, we now extend the analysis to resolve vertical heterogeneity. A distributed TRT employs DTS to record temperature variations along a borehole during the field test, enabling depth-specific characterization of ground thermal properties [49]. This method permits estimation of ground thermal conductivity and borehole thermal resistance as functions of depth, contributing to a more detailed assessment of subsurface conditions. The vertical profiles of thermal conductivity k_s and volumetric heat capacity C_s derived from the CCS formulation, as well as the ILS and ICSS approaches, are presented in Fig. 10. The RMSE across 54 individual inversions is 0.116 °C for the CCS solution, 0.163 °C for the ILS solution, and 8.73 °C for the ICSS solution. Given that the RMSE of the ICSS solution is approximately two orders of magnitude higher, it is excluded from further consideration.

The CCS solution resolves modest but systematic vertical stratification. Thermal conductivity increases gradually from 0.90 Wm^{-1} °C^{-1} at 5 m to approximately 1.05 W m^{-1} °C^{-1} at 50 m, with local minima at 6 m, 17 m, and 29 m corresponding to silt–clay interbeds identified in borehole cuttings. In the clay-with-gravel-and-cobbles interval between roughly 23 m and 32 m, the profile exhibits the opposite trend where k_s increases while C_s decreases, analogous to the typical behavior of hydraulic conductivity rising as specific storage declines in coarser, better-drained materials [50]. Overall, C_s increases from approximately 2.0×10^6 J m^{-3} °C^{-1} near the surface to 3.4×10^6 J m^{-3} °C^{-1} at depth, consistent with the effects of increasing overburden pressure, greater bulk density, and higher water saturation in deeper sand–gravel units. In contrast, the ILS inversion produces nearly uniform values of $k_s = 1.25$ Wm^{-1} °C^{-1} and $C_s = 1.5 \times 10^6$ J m^{-3} °C^{-1} along the borehole, overestimating conductivity and underestimating heat capacity relative to both the CCS estimates and laboratory needle-probe data. Because the ILS model neglects grout heat storage, it compensates by inflating k_s during the early heating phase (Fig. 10a), which subsequently leads to underestimation of C_s at later times (Fig. 10b).

The inferred grout heat-capacity profile shown in Fig. 11, while broadly uniform at approximately $1.3–1.7 \times 10^6$ J m^{-3} °C^{-1}, exhibits minor deviations from flatness. A gradual increase between 20 m and 35 m aligns with a borehole enlargement indicated by caliper logs and cuttings; this localized widening would accommodate more backfill per meter, yielding a moderate increase in

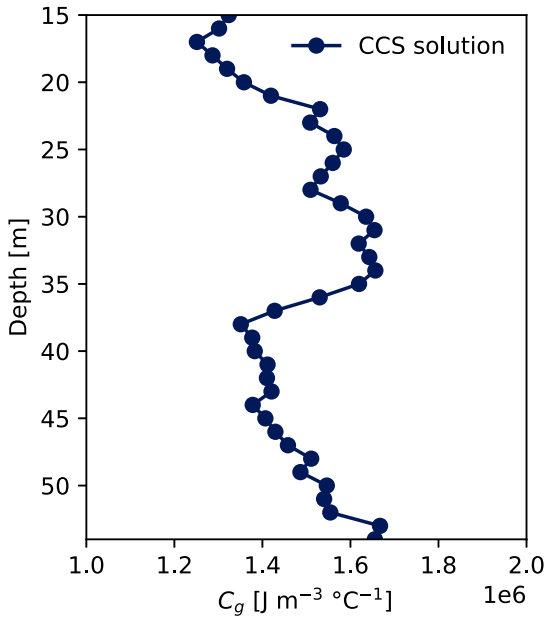

Fig. 11. Grout/backfill volumetric heat-capacity profile C_g obtained with the proposed CCS model (Eq. (23)).

bulk grout mass and thus higher C_g. Shallower undulations, within ±10% of the mean, may arise from density variations during tremie-grouting, segregation or bleed-water loss, or drilling-induced wellbore skin effects that modify thermal contact between grout and formation. Although these variations are minor relative to the average, they are unlikely to influence depth-averaged TRT interpretation. Nonetheless, their distinct expression in the DTS-based inversion highlights the sensitivity of the CCS framework to subtle near-borehole heterogeneity.

Overall, the distributed TRT confirms that the test site is only mildly heterogeneous and that apparent model differences dominate over genuine stratigraphic variability when grout heat storage is neglected. Nevertheless, the CCS model ability to resolve meter-scale variations in all three parameters while retaining the lowest RMSE underscores the practical value of including grout capacity in the inner boundary condition of analytical TRT solutions.

3.5. Performance summary, limitations, and practical implications

To synthesize the findings from both the theoretical benchmarking and the field application, Table 3 presents a comprehensive comparison of the ILS, ICSS, and CCS models. This evaluation considers physical validity, computational efficiency, ease of use, and quantitative accuracy based on the field test results.

While the ILS and ICSS models offer high computational speed, they suffer from significant limitations in physical accuracy, particularly during the early heating phase. The ILS model systematically underestimates the temperature rise (RMSE = 0.16 °C), while the ICSS model overestimates it (RMSE = 0.25 °C) due to the neglect of grout heat capacity. In contrast, the proposed CCS model achieves the highest accuracy (RMSE = 0.12 °C) by physically resolving the grout thermal mass. Crucially, this gain in accuracy does not come at the cost of usability; the CCS model retains a closed-form analytical structure that is computationally efficient and easy to implement in standard engineering workflows.

Despite its demonstrated accuracy, the current CCS model relies on assumptions that define its validity range. First, the model assumes radial homogeneity beyond the borehole wall. While the depth-resolved analysis (Fig. 10) successfully captures vertical stratification by treating each depth slice independently, strong radial heterogeneities or significant groundwater advection would require extending the kernel to a moving source or composite-medium formulation. Second, vertical heat transfer is assumed to be negligible. This assumption is valid for deep boreholes ($L \gg r_b$) and short-to-medium test durations where the thermal diffusion length remains small relative to the borehole depth. However, for very shallow systems or tests extending over extremely long periods, end effects may become significant, necessitating a 2D finite-line source correction. Future work will focus on incorporating these factors while retaining the computational efficiency of the analytical framework.

4. Conclusion

This study develops the CCS analytical TRT solution, which reproduces Laplace-transform finite-difference benchmarks within the accuracy of 0.1 °C. The model's validity was further confirmed against rigorous two-zone numerical benchmarks, proving the robustness of the lumped-capacity assumption. Field application demonstrates that the CCS model reduces depth-resolved RMSE

Table 3
Comprehensive comparison of the ILS, ICSS, and CCS models based on theoretical characteristics and field performance.

Metric	ILS model	ICSS model	CCS model (Proposed)
Physical Validity			
Geometry	Line Source	Hollow Cylinder	**Solid Cylinder**
Grout Capacity (C_g)	Neglected	Neglected	**Included**
Performance (Field)			
Early-time Bias	Underestimation	Overestimation	**Minimal**
RMSE (Depth-Avg.) (°C)	0.16	0.25	0.12
RMSE (Depth-Resolved) (°C)	0.163	8.73	0.116
Practicality			
Computational Speed	Very High	High	High
Ease of Use	High	Moderate	**Moderate**

to 0.116 °C, compared with 0.163 °C for the ILS and more than 8 °C for the ICSS (Fig. 8). By embedding grout volumetric heat capacity in a closed-form G-function, the model resolves meter-scale variations in k_s, C_s, and C_g consistent with borehole lithology, indicating that storage effects can be separated from stratigraphic heterogeneity.

Bayesian uncertainty analysis revealed a 'decoupling peak' in parameter uncertainty at approximately 42 h, marking the physical transition from grout- to ground-dominated heat transfer. Tests shorter than this duration risk false convergence. However, immediately following this peak, the weighted uncertainty drops to engineering-acceptable levels (<15%) by 48–50 h. This identifies a practical optimal test duration that ensures physical robustness while offering significant time savings compared to the conventional 72 h requirement.

Because the current axisymmetric formulation neglects vertical conduction, caution is required for shallow boreholes or sites affected by surface-temperature variability. Future work will include vertical heat flux, radial heterogeneity, and groundwater advection, and will integrate the kernel into real-time Bayesian inversion to further reduce field-test duration and accelerate deployment of ground-coupled energy systems.

CRediT authorship contribution statement

Hsiang-Wen Wang: Writing – original draft, Visualization, Software, Formal analysis, Conceptualization. **Ying-Fan Lin:** Writing – review & editing, Writing – original draft, Visualization, Validation, Supervision, Software, Methodology, Conceptualization. **Chia-Hao Chang:** Methodology, Data curation. **Bo-Tsen Wang:** Methodology, Data curation. **Hikari Fujii:** Writing – review & editing, Methodology. **Yu-Feng Forrest Lin:** Writing – review & editing, Validation. **Kuo-Hsin Yang:** Supervision, Methodology. **Jui-Pin Tsai:** Writing – review & editing, Validation, Supervision, Resources, Methodology, Funding acquisition, Formal analysis, Conceptualization.

Declaration of competing interest

The authors declare that they have no known competing financial interests or personal relationships that could have appeared to influence the work reported in this paper.

Acknowledgments

The authors express their sincere gratitude to the Associate Editor, Prof. Dong Rip Kim, and the three anonymous reviewers for their constructive comments and suggestions, which have significantly improved the quality of this manuscript. Ying-Fan Lin thanks the John Su Foundation for supporting this study. This study is supported by grants from the Taiwan National Science and Technology Council under the contract numbers 113-2222-E-033-002-MY2, 114-2221-E-033-005, 113-2221-E-002-160, and 113-2811-E-002-061.

Data availability

Data will be made available on request.

References

[1] C. Brown, I. Kolo, A. Lyden, L. Franken, N. Kerr, D. Marshall-Cross, S. Watson, G. Falcone, D. Friedrich, J. Diamond, Assessing the technical potential for underground thermal energy storage in the UK, Renew. Sustain. Energy Rev. 199 (2024) 114545, http://dx.doi.org/10.1016/j.rser.2024.114545.

[2] F. Guo, X. Zhu, P. Li, X. Yang, Low-grade industrial waste heat utilization in urban district heating: Simulation-based performance assessment of a seasonal thermal energy storage system, Energy 239 (2022) 122345, http://dx.doi.org/10.1016/j.energy.2021.122345.

[3] P. Adebayo, C.B. Jathunge, A. Darbandi, N. Fry, R. Shor, A. Mohamad, C. Wemhöner, A. Mwesigye, Development, modeling, and optimization of ground source heat pump systems for cold climates: A comprehensive review, Energy Build. 320 (2024) 114646, http://dx.doi.org/10.1016/j.enbuild.2024.114646.

[4] H. Skarphagen, D. Banks, B.S. Frengstad, H. Gether, Design considerations for borehole thermal energy storage (BTES): A review with emphasis on convective heat transfer, Geofluids 2019 (1) (2019) 4961781, http://dx.doi.org/10.1155/2019/4961781.

[5] G. Hou, H. Taherian, Y. Song, W. Jiang, D. Chen, A systematic review on optimal analysis of horizontal heat exchangers in ground source heat pump systems, Renew. Sustain. Energy Rev. 154 (2022) 111830, http://dx.doi.org/10.1016/j.rser.2021.111830.

[6] E.D. Kerme, A.S. Fung, M.Z. Saghir, Performance optimization of double U-tube borehole heat exchanger for thermal energy storage, Energy Storage 7 (2) (2025) e70145, http://dx.doi.org/10.1002/est2.70145.

[7] M. King, C.-Y. Yune, Advanced machine learning techniques: Forecasting thermal resistance in borehole heat exchanger system through RSM and hybrid DFNN-GA approaches, Geothermics 120 (2024) 103004, http://dx.doi.org/10.1016/j.geothermics.2024.103004.

[8] H. Sadeghi, R. Jalali, R.M. Singh, A review of borehole thermal energy storage and its integration into district heating systems, Renew. Sustain. Energy Rev. 192 (2024) 114236, http://dx.doi.org/10.1016/j.rser.2023.114236.

[9] A.A. Serageldin, K. Nagano, A novel oscillatory thermal response test method for efficient characterization of ground thermal properties: Methodology and data analysis, Renew. Energy 230 (2024) 120674, http://dx.doi.org/10.1016/j.renene.2024.120674.

[10] Y. Zhao, H. Wang, X. Li, Field test on the thermal performance of double-layer pipe-embedded wall heating system with shallow geothermal energy and air source heat pump, Appl. Energy 377 (2025) 124676, http://dx.doi.org/10.1016/j.apenergy.2024.124676.

[11] P. Mogensen, Fluid to duct wall heat transfer in duct system heat storages, Doc.-Swedish Counc. Build. Res. (16) (1983) 652–657.

[12] J.C. Jaeger, H.S. Carslaw, Conduction of heat in solids, in: P. Clarendon (Ed.), Transport Phenomena in Materials Processing, Springer, Cham, Switzerland, 1959, pp. 281–327, http://dx.doi.org/10.1007/978-3-319-48090-9_9.

[13] P. Pasquier, L. Lamarche, Analytic expressions for the moving infinite line source model, Geothermics 103 (2022) 102413, http://dx.doi.org/10.1016/j.geothermics.2022.102413.

[14] D. Gordon, T. Bolisetti, D.S.-K. Ting, S. Reitsma, Short-term fluid temperature variations in either a coaxial or U-tube borehole heat exchanger, Geothermics 67 (2017) 29–39, http://dx.doi.org/10.1016/j.geothermics.2016.12.001.

[15] M. Li, A.C. Lai, Review of analytical models for heat transfer by vertical ground heat exchangers (GHEs): A perspective of time and space scales, Appl. Energy 151 (2015) 178–191, http://dx.doi.org/10.1016/j.apenergy.2015.04.070.

[16] S. Gehlin, Thermal Response Test: Method Development and Evaluation (Ph.D. thesis), Luleå tekniska universitet, 2002.

[17] J.D. Spitler, S.E. Gehlin, Thermal response testing for ground source heat pump systems—An historical review, Renew. Sustain. Energy Rev. 50 (2015) 1125–1137.

[18] N. Molina-Giraldo, P. Blum, K. Zhu, P. Bayer, Z. Fang, A moving finite line source model to simulate borehole heat exchangers with groundwater advection, Int. J. Therm. Sci. 50 (12) (2011) 2506–2513, http://dx.doi.org/10.1016/j.ijthermalsci.2011.06.012.

[19] H.Y. Zeng, N.R. Diao, Z.H. Fang, A finite line-source model for boreholes in geothermal heat exchangers, Heat Transf. 31 (7) (2002) 558–567, http://dx.doi.org/10.1002/htj.10057.

[20] Y. Zhou, Z.-h. Wu, K. Wang, An analytical model for heat transfer outside a single borehole heat exchanger considering convection at ground surface and advection of vertical water flow, Renew. Energy 172 (2021) 1046–1062, http://dx.doi.org/10.1016/j.renene.2021.03.102.

[21] A.J. Extremera-Jiménez, C. Yousif, P.J. Casanova-Peláez, F. Cruz-Peragón, Fast segregation of thermal response functions in short-term for vertical ground heat exchangers, Appl. Therm. Eng. 246 (2024) 122849, http://dx.doi.org/10.1016/j.applthermaleng.2024.122849.

[22] M. Mahmoud, M. Ramadan, K. Pullen, M.A. Abdelkareem, T. Wilberforce, A.-G. Olabi, S. Naher, A review of grout materials in geothermal energy applications, Int. J. Thermofluids 10 (2021) 100070, http://dx.doi.org/10.1016/j.ijft.2021.100070.

[23] R.A. Beier, Analysis of thermal response tests on boreholes with controlled inlet temperature versus controlled heat input rate, Geothermics 94 (2021) 102099, http://dx.doi.org/10.1016/j.geothermics.2021.102099.

[24] C. Wang, W. Sun, Q. Fu, Y. Lu, P. Zhang, Semi-analytical and numerical modeling of U-bend deep borehole heat exchanger, Renew. Energy 222 (2024) 119959, http://dx.doi.org/10.1016/j.renene.2024.119959.

[25] Y. Man, H. Yang, N. Diao, J. Liu, Z. Fang, A new model and analytical solutions for borehole and pile ground heat exchangers, Int. J. Heat Mass Transfer 53 (13–14) (2010) 2593–2601, http://dx.doi.org/10.1016/j.ijheatmasstransfer.2010.03.001.

[26] L. Lamarche, B. Beauchamp, New solutions for the short-time analysis of geothermal vertical boreholes, Int. J. Heat Mass Transfer 50 (7–8) (2007) 1408–1419.

[27] S. Javed, J. Claesson, New analytical and numerical solutions for the short-term analysis of vertical ground heat exchangers, ASHRAE Trans. 117 (1) (2011) 3–12.

[28] A. Priarone, M. Fossa, Temperature response factors at different boundary conditions for modelling the single borehole heat exchanger, Appl. Therm. Eng. 103 (2016) 934–944, http://dx.doi.org/10.1016/j.applthermaleng.2016.04.038.

[29] M.D. Morris, Factorial sampling plans for preliminary computational experiments, Technometrics 33 (2) (1991) 161–174, http://dx.doi.org/10.2307/1269043.

[30] P. Eskilson, Thermal analysis of heat extraction boreholes, 1987.

[31] G. Hellström, Ground Heat Storage: Thermal Analyses of Duct Storage Systems. I. Theory (Ph.D. thesis), Lund University, Department of Mathematical Physics, Lund, Sweden, 1991, URL: https://lup.lub.lu.se/search/files/6178678/8161230.pdf. Doctoral Thesis (monograph).

[32] I.S. Papadopulos, H.H. Cooper Jr., Drawdown in a well of large diameter, Water Resour. Res. 3 (1) (1967) 241–244, http://dx.doi.org/10.1029/WR003i001p00241.

[33] L.N. Trefethen, J.A.C. Weideman, The exponentially convergent trapezoidal rule, SIAM Rev. 56 (3) (2014) 385–458, http://dx.doi.org/10.1137/130932132.

[34] J.A. Shonder, J.V. Beck, Field test of a new method for determining soil formation thermal conductivity and borehole resistance, Technical Report, Oak Ridge National Lab., TN (US), 2000.

[35] L.R. Ingersoll, O.J. Zobel, A.C. Ingersoll, Heat Conduction with Engineering, Geological, and Other Applications, McGraw–Hill, New York, 1954.

[36] H. Stehfest, Algorithm 368: Numerical inversion of Laplace transforms [D5], Commun. ACM 13 (1) (1970) 47–49.

[37] G.J. Moridis, D.L. Reddell, The Laplace transform finite difference method for simulation of flow through porous media, Water Resour. Res. 27 (8) (1991) 1873–1884, http://dx.doi.org/10.1029/91WR01190.

[38] I.M. Sobol, Global sensitivity indices for nonlinear mathematical models and their Monte Carlo estimates, Math. Comput. Simulation 55 (1–3) (2001) 271–280.

[39] A. Saltelli, M. Ratto, T. Andres, F. Campolongo, J. Cariboni, D. Gatelli, M. Saisana, S. Tarantola, Global Sensitivity Analysis: the Primer, John Wiley & Sons, 2008.

[40] N. Van De Giesen, S.C. Steele-Dunne, J. Jansen, O. Hoes, M.B. Hausner, S. Tyler, J. Selker, Double-ended calibration of fiber-optic Raman spectra distributed temperature sensing data, Sensors 12 (5) (2012) 5471–5485, http://dx.doi.org/10.3390/s120505471.

[41] S.-O. Chung, R. Horton, Soil heat and water flow with a partial surface mulch, Water Resour. Res. 23 (12) (1987) 2175–2186, http://dx.doi.org/10.1029/WR023i012p02175.

[42] N. Diao, Q. Li, Z. Fang, Heat transfer in ground heat exchangers with groundwater advection, Int. J. Therm. Sci. 43 (12) (2004) 1203–1211, http://dx.doi.org/10.1016/j.ijthermalsci.2004.04.009.

[43] M. Taussi, W. Borghi, M. Gliaschera, A. Renzulli, Defining the shallow geothermal heat-exchange potential for a lower fluvial plain of the central apennines: The Metauro Valley (Marche region, Italy), Energies 14 (3) (2021) 768, http://dx.doi.org/10.3390/en14030768.
[44] B.L. Kurylyk, K.T. MacQuarrie, D. Caissie, J.M. McKenzie, Shallow groundwater thermal sensitivity to climate change and land cover disturbances: derivation of analytical expressions and implications for stream temperature modeling, Hydrol. Earth Syst. Sci. 19 (5) (2015) 2469–2489, http://dx.doi.org/10.5194/hess-19-2469-2015.
[45] R. Storn, K. Price, Differential evolution–a simple and efficient heuristic for global optimization over continuous spaces, J. Global Optim. 11 (1997) 341–359, http://dx.doi.org/10.1023/A:1008202821328.
[46] F. Loveridge, W. Powrie, Temperature response functions (G-functions) for single pile heat exchangers, Energy 57 (2013) 554–564, http://dx.doi.org/10.1016/j.energy.2013.04.060.
[47] A. McDaniel, J. Tinjum, D.J. Hart, Y.-F. Lin, A. Stumpf, L. Thomas, Distributed thermal response test to analyze thermal properties in heterogeneous lithology, Geothermics 76 (2018) 116–124, http://dx.doi.org/10.1016/j.geothermics.2018.07.003.
[48] H. Liu, A.J. Stumpf, Y.-F.F. Lin, X. Liu, Distributed thermal response multi-source modeling to evaluate heterogeneous subsurface properties, Groundwater 61 (2) (2023) 224–236, http://dx.doi.org/10.1111/gwat.13154.
[49] H. Fujii, H. Okubo, K. Nishi, R. Itoi, K. Ohyama, K. Shibata, An improved thermal response test for U-tube ground heat exchanger based on optical fiber thermometers, Geothermics 38 (4) (2009) 399–406, http://dx.doi.org/10.1016/j.geothermics.2009.06.002.
[50] J.A. Cherry, R.A. Freeze, Groundwater, Prentice-Hall, Englewood Cliffs, NJ, 1979.